

DOES THE CHEMOTHERMAL INSTABILITY HAVE ANY ROLE IN THE FRAGMENTATION OF  
PRIMORDIAL GAS

JAYANTA DUTTA

Department of Physics, Indian Institute of Science, Bangalore-560012, India  
email: jd.astrop@gmail.com*Draft version March 6, 2022*

## ABSTRACT

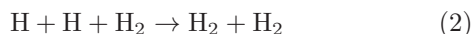
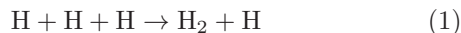
The collapse of the primordial gas in the density regime  $\sim 10^8\text{--}10^{10}\text{ cm}^{-3}$  is controlled by the three-body  $\text{H}_2$  formation process, in which the gas can cool faster than free-fall time – a condition proposed as the chemothermal instability. We investigate how the heating and cooling rates are affected during the rapid transformation of atomic to molecular hydrogen. With a detailed study of the heating and cooling balance in a 3D simulation of Pop III collapse, we follow the chemical and thermal evolution of the primordial gas in two dark matter minihaloes. The inclusion of sink particles in modified Gadget-2 smoothed particle hydrodynamics code allows us to investigate the long term evolution of the disk that fragments into several clumps. We find that the sum of all the cooling rates is less than the total heating rate after including the contribution from the compressional heating ( $p dV$ ). The increasing cooling rate during the rapid increase of the molecular fraction is offset by the unavoidable heating due to gas contraction. We conclude that fragmentation occurs because  $\text{H}_2$  cooling, the heating due to  $\text{H}_2$  formation and compressional heating together set a density and temperature structure in the disk that favors fragmentation, not the chemothermal instability.

*Subject headings:* stars: formation – stars: early universe – hydrodynamics – instabilities

## 1. INTRODUCTION

Understanding the first source of light in the Universe, the so-called primordial stars or Population III (Pop III) stars, is crucial in determining how the Universe evolved into what we observe today (Bromm & Yoshida 2011; Bromm 2013; Glover 2013). With the help of state-of-the-art simulations along with the well established cosmological parameter (Planck Collaboration et al. 2014), recent studies have provided a standard model of the Pop III star formation (e.g., Greif et al. 2012; Johnson et al. 2013; Stacy et al. 2013; Hirano et al. 2014, 2015; Hartwig et al. 2015). In this picture, the baryons (mainly atomic hydrogen) in low mass ( $\sim 10^5\text{--}10^6 M_\odot$ ) dark matter halo with virial temperature  $\sim 1000\text{ K}$  gravitationally collapsed at redshift  $z \geq 20$  via  $\text{H}_2$  molecular cooling to form the very first stars in the Universe (Haiman et al. 1996; Tegmark et al. 1997; Barkana & Loeb 2001; Bromm & Larson 2004; Ciardi & Ferrara 2005).

Initially the gas is cooled via  $\text{H}_2$  rotational and vibrational line emission (Susa et al. 1998; Omukai & Nishi 1998). However, the quick conversion of atomic hydrogen into molecules via the three-body reactions (Palla et al. 1983):



can cool the gas rapidly at high densities ( $\sim 10^8\text{ cm}^{-3}$ ). This results in the gas to be chemothermally unstable (Yoshida et al. 2006; Turk et al. 2009). The physical processes are extremely complex during the three-body reaction. The gas undergoes both heating and cooling simultaneously. Heating is due to the release of 4.4 eV energy associated with every  $\text{H}_2$  formation and gas con-

traction, and cooling is due to the emission, dissociation of  $\text{H}_2$  and collisions of  $\text{H}_2$ . However, there is little understanding of the interplay between the heating and cooling rates so far.

In addition, the physics at high densities is relevant to the inception of the thermal instability (first predicted by e.g., Sabano & Yoshii 1977; Silk 1983) that can generate fluctuations in the gas density in a comparatively shorter interval than the collapse time. The numerical simulations by Abel et al. (2002) found several chemothermally unstable regions. They have, however, pointed out that the instabilities do not lead to fragmentation as the turbulence efficiently mixes the gas, thereby erasing the fluctuations before they can grow significantly. In a different approach, Omukai & Yoshii (2003) have calculated the stability of the gas cloud for isobaric perturbations by introducing the ‘growth parameter ( $Q$ )’, which must be significantly larger than unity for a clump of gas to break into multiple objects. A detailed analytical calculation of the instability criterion has been investigated by Ripamonti & Abel (2004). The high resolution 3D  $\Lambda$ CDM cosmological simulation by Yoshida et al. (2006) has shown that the growth parameter indeed never becomes much larger than unity. It is in fact less than 1.5, which implies that the chemothermal instability cannot lead to any fragmentation. A similar conclusion was drawn by Turk et al. (2009). In contrast, more recently Greif et al. (2013) have used *Arepo* simulations to follow the evolution of the gas in minihaloes that fragments. They have suggested that this is due to the chemothermal instability because the ratio of the cooling timescale to the free-fall timescale drops below unity in the density space where the three-body reaction dominates.

Our approach to study the chemothermal instability as the sole reason for fragmentation scenarios is significantly

different from those in the previous works. For example, for the first time to the best of our knowledge, we investigate the heating and cooling balance in a full 3D simulation of Pop III collapse to understand better the physical processes during the rapid conversion of atomic to molecular hydrogen. The closest study so far would be the analysis by Omukai et al. (2005). However, they examined idealised 1D collapse models without exploring the uncertainties in the three-body rates. In this paper, we investigate the chemothermal instability by comparing different heating and cooling rates and discuss their roles in the fragmentation during the long-term evolution of the disk.

## 2. NUMERICAL METHODOLOGY

The simulation setup and initial conditions are similar to our previous study (Dutta et al. 2015) that used minihaloes from the cosmological simulations of Greif et al. (2011). Both the haloes start with a maximum central cloud number density  $n \sim 10^6 \text{ cm}^{-3}$ , the density before the onset of the three-body reaction. The details of the halo properties are given in Table 1. We use the halo configurations as the initial condition for our standard SPH code Gadget-2 (Springel 2005) that has been modified with the inclusion of sink particles (Bate et al. 1995; Jappsen et al. 2005) and time-dependent chemical network for primordial gas (Clark et al. 2011a). The snapshots from the hydrodynamic moving mesh code *Arepo* (Springel 2010) are converted into the Gadget-2 implementation (Smith et al. 2011). This is possible because the mesh-generating points of *Arepo* can be interpreted as the Lagrangian fluid particles. The mass resolution in our Gadget-2 simulation is  $\approx 10^{-2} M_\odot$  for 100 SPH particles (Bate & Burkert 1997).

Once the gas density reaches  $\sim 10^{10} \text{ cm}^{-3}$ , the cloud becomes opaque and the strongest of  $\text{H}_2$  lines becomes optically thick. The  $\text{H}_2$  cooling rate in this regime is calculated using the Sobolev approximation (as described in Yoshida et al. 2006). At densities  $\geq 10^{14} \text{ cm}^{-3}$ , the gas goes through a phase of cooling instability due to rapid increase in the cooling rate by  $\text{H}_2$  collisional induced emission (CIE). We follow Ripamonti & Abel (2004) to use the rate in our cooling function. Above the central density  $\sim 10^{16} \text{ cm}^{-3}$ , the gas becomes completely optically thick to the continuum radiation (Yoshida et al. 2008). At this point, the remaining  $\text{H}_2$  dissociates by collisions with the atomic H and other  $\text{H}_2$  molecules, and consequently cools the gas resulting in further collapse.

We ensure that our investigation is not biased on the chemical uncertainties and halo configuration. Hence, we simulate the gas evolution in two different minihaloes with the extreme three-body rate coefficients: Abel et al. (2002) (hereafter ABN02) provide the slowest rate, Flower & Harris (2007) (hereafter FH07) provide the fastest rate. Using the highly simplified one-zone models, the works by Glover & Abel (2008) and Glover & Savin (2009) examined minutely the effects of the uncertainty in the three-body  $\text{H}_2$  formation rates and the cooling rate on the thermal evolution of the collapsing gas in simple Bonnor-Ebert spheres (Ebert 1955; Bonnor 1956). They have found that the large uncertainty between the ABN02 and FH07, which differ by a large amount, lead to an uncertainty of approximately 50% in the temperature evolution of the gas in the density

Halo properties	halo1	halo2
$n \text{ (cm}^{-3}\text{)}$	$10^6 \text{ (max) } 71 \text{ (min)}$	$10^6 \text{ (max) } 85 \text{ (min)}$
$T \text{ (K)}$	$469 \text{ (max) } 59 \text{ (min)}$	$436 \text{ (max) } 54 \text{ (min)}$
mass ( $M_\odot$ )	1030	1093
n-SPH	690855	628773
resolution ( $M_\odot$ ) for 100 n-SPH	$1.3 \times 10^{-2}$	$1.4 \times 10^{-2}$

TABLE 1  
SUMMARY OF MINIHALOS FROM THE COSMOLOGICAL SIMULATIONS.  
N-SPH STANDS FOR THE NUMBER OF SPH PARTICLES IN THE SIMULATION.

range  $10^8 < n < 10^{13} \text{ cm}^{-3}$ .

The primordial protostar can be modeled as a sink particle (Krumholz et al. 2004), which basically replaces the high-density region as a protostar that can accrete infalling mass. In our simulations, the protostar is formed once the number density of the gas reaches  $5 \times 10^{13} \text{ cm}^{-3}$  and temperature is  $\sim 1000 \text{ K}$ . The Jeans mass at this critical point is  $M_J (1000 \text{ K}, 10^{13} \text{ cm}^{-3}) \sim 0.06 M_\odot$  and Jeans radius is 6 AU, which is the accretion radius,  $r_{\text{acc}}$ , of the sink particle. The spurious formation of new sink particles is avoided by preventing the sink particles from forming within  $2r_{\text{acc}}$  of one another. Depending on the halo configurations and chemical uncertainties, our simulations run  $\approx 3500\text{--}6500 \text{ yr}$  after the formation of the first protostar.

## 3. RESULTS

### 3.1. Chemothermal instability

As the gas undergoes gravitational collapse, the crucial aspect to be investigated is whether the gas will be able to cool significantly or not. The rapid formation of hydrogen molecules via three-body reactions allows the gas to cool in less than a free-fall time, heralding chemothermal instability. This effect for both the ABN02 and FH07 rates has been shown by Dutta et al. (2015), where we have found that the ratio of the cooling time to the free-fall time ( $t_{\text{cool}}/t_{\text{ff}}$ ) dips below unity at a certain density. This is exactly what Greif et al. (2013) have found in their simulations. In our present calculation, we have considered all the cooling mechanisms, including the contributions from chemical heating, to calculate the cooling time:  $t_{\text{cool}} = \epsilon/\Lambda_{\text{net}}$ , where  $\epsilon$  is the energy per unit volume of the gas and  $\Lambda_{\text{net}}$  is the net cooling rate in units of  $\text{erg s}^{-1} \text{ cm}^{-3}$ . This implies that the gas can cool as it collapses, and is hence undergoing chemothermal instability. It is to be noted that the drop in the ratio  $t_{\text{cool}}/t_{\text{ff}}$  coincides with the onset (in density space) of the three-body  $\text{H}_2$  formation (Greif et al. 2013; Dutta et al. 2015).

However, as we have discussed in Section 1, there is still some discrepancy of whether the fragmentation is stimulated by the chemothermal instability or not. Fragmentation might also depend on other details, such as turbulence, rotation, etc (see for examples, Turk et al. 2009; Stacy et al. 2010; Clark et al. 2011b; Latif et al. 2015; Dutta 2015). The variation of the ratio of the cooling time to the free-fall time in the density space, where the three-body reactions take place, is too simple to make a definite conclusion about the fragmentation. A straightforward analysis involves comparing all possible heating and cooling processes that are responsible for

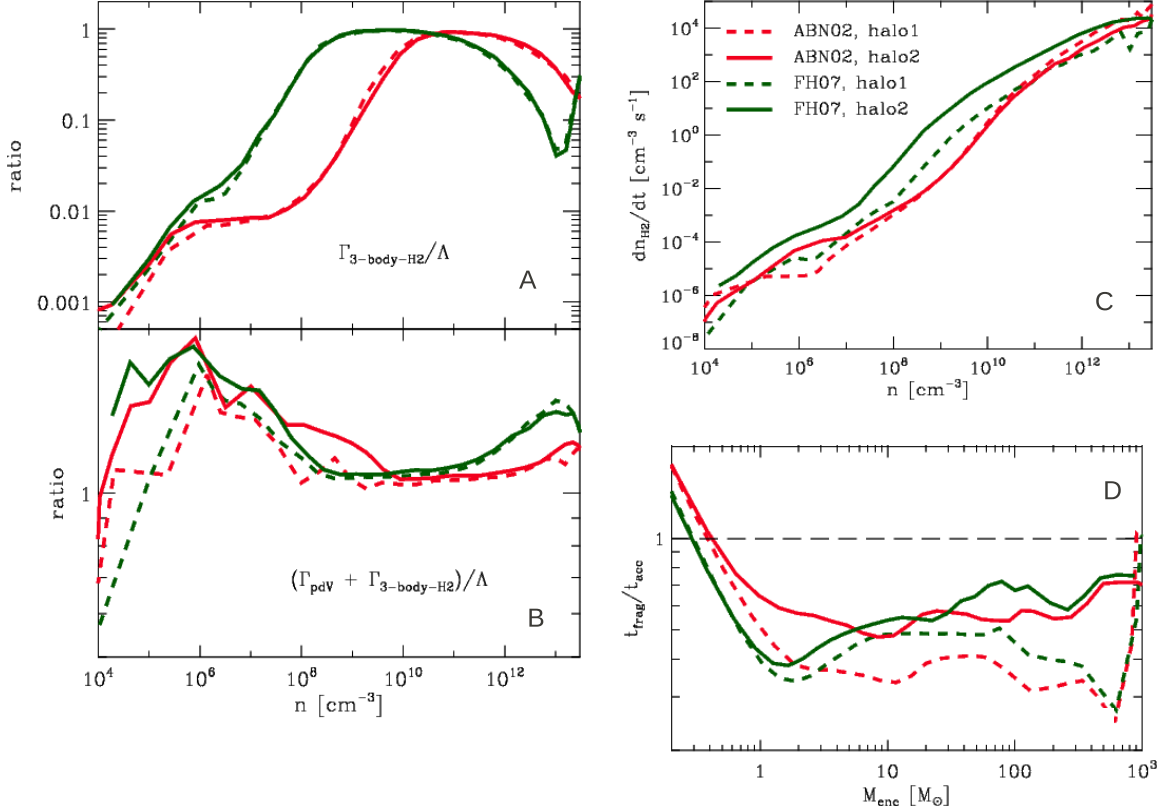


FIG. 1.— Radially binned, mass-weighted averages of the physical quantities for different proposed three-body  $\text{H}_2$  formation rates (red: ABN02, green: FH07) of two cosmological halos (dotted: halo1, solid: halo2) are compared just before the first protostar is formed. (A) The ratio of the three-body formation heating to the total cooling rate, (B) ratio of the total heating to the total cooling rate and (C) the rate of  $\text{H}_2$  formation ( $dn_{\text{H}_2}/dt$ ) from the simulations in the units of  $\text{cm}^{-3} \text{s}^{-1}$  are plotted as a function of density. (D) The fragmentation time over the accretion time is plotted as a function of enclosed gas mass.

setting the thermal balance in the gas.

### 3.2. Heating and Cooling rates

In this section, we investigate the relevant cooling and heating mechanisms associated with the emission, chemical reaction and gas contraction during collapse. The synchronous effects of the cooling and heating rates make the chemical and thermodynamical evolution complicated.

Assuming the evolution of the gas density ( $\rho$ ) with the free-fall time ( $t_{\text{ff}}$ ), i.e.,  $d\rho/dt = \rho/t_{\text{ff}}$ , previous studies (e.g., Omukai 2000; Bromm et al. 2002) show that the thermal evolution is followed by solving the energy equation:

$$\frac{d\epsilon}{dt} = \frac{p}{\rho} \frac{d\rho}{dt} - \Lambda + \Gamma, \quad (3)$$

where  $\Lambda$  and  $\Gamma$  are the cooling and heating rate respectively in units of  $\text{erg s}^{-1} \text{cm}^{-3}$ . This can be seen in Figure 1 in which we compare the various heating and cooling rates in the simulation as a function of density. All the quantities are mass-weighted averages of the individual SPH particles that are binned logarithmically in radius. These logarithmic-binned spherical shells are centered at the origin at  $r = 0$ . We have rigorously verified that the mass-weighted averaging does not throw away any physical information. The calculations are done once the central region has collapsed to a density  $\sim 5 \times 10^{13}$

$\text{cm}^{-3}$ , i.e., just before the formation of the first sink.

We take the total cooling rate as the sum of the  $\text{H}_2$  line-cooling rate, collision induced emission cooling rate (CIE) and dissociation rate (i.e.  $\Lambda = \Lambda_{\text{line}} + \Lambda_{\text{CIE}} + \Lambda_{\text{Diss}}$ ) and total heating rate as the combination of heating from the compression ( $pdV$ ) and the three-body formation of  $\text{H}_2$  (i.e.  $\Gamma = \Gamma_{\text{pdV}} + \Gamma_{3\text{-body-H}_2}$ ).

Figure 1A shows that the total cooling can be as high as the heating associated with the three-body formation of  $\text{H}_2$ , and thus the ratio of  $\Gamma_{3\text{-body-H}_2}$  to  $\Lambda$  is of order unity in the density space where the three-body reaction dominates. The three-body heating rates for the FH07 rise before the ABN02 do because the higher  $\text{H}_2$  formation rates of FH07 cause the gas to become fully molecular at lower densities. As a result, the gas in the FH07 case becomes optically thick at earlier times, preventing the thermal energy from being transported efficiently out of the disk. We have verified that other cooling processes, such as the heat loss due to the collisional dissociation or the collision induced emission are not effective until much higher densities.

Most importantly, when including the contribution from compressional heating, we notice that the total heating rate is always greater than the total cooling rate of the gas (Figure 1B). For the gas to be chemothermally unstable to fragmentation, the heating and cooling rate

must satisfy the condition:

$$\Lambda_{\text{line}} + \Lambda_{\text{CIE}} + \Lambda_{\text{Diss}} \geq \Gamma_{\text{pdV}} + \Gamma_{\text{3-body-H2}}, \quad (4)$$

that could occur due to a sharp increase in the fractional abundances. However, in our case, the total heating rate dominates even in the high density regime. This leads to an ever increasing temperature with density.

From this analysis, we tentatively conclude that the gas can experience a dip in the ratio of the cooling time to the free-fall time in the density space, and hence becomes chemothermally unstable. However, the rapid cooling due to the three-body reaction is counterbalanced by the compressional heating. Thus it never leads to significant drop in the temperature. This is consistent with the previous studies (e.g., Abel et al. 2002; Bromm et al. 2002; Ripamonti & Abel 2004; Yoshida et al. 2006).

At this point, we would like to point out the differences with the work by Greif et al. (2013). The use of the ratio  $t_{\text{cool}}/t_{\text{ff}}$  as a criterion for fragmentation and collapse by Greif et al. (2013) neglects the heating due to the formation of  $\text{H}_2$  and  $\text{pdV}$  contraction. This heating generally exceeds  $\text{H}_2$  cooling and dominates the temperature and density evolution of the collapsing gas, and hence its tendency to fragment and form new stars.

Another point to note is that a change in the analysis of the ratio,  $t_{\text{cool}}/t_{\text{ff}}$ , does not necessarily coincide with a change in the ratio of the free-fall time to the sound crossing time – which is a measure of the number of Jeans masses. Note that Turk et al. (2009) were the first to find the fragmentation in the Pop III star forming haloes because they included the heating due to  $\text{H}_2$  formation, whereas Yoshida et al. (2008) did not. These studies along with our detailed rigorous analysis support the claims that the contribution from both the three-body  $\text{H}_2$  formation heating and compressional heating must be included to capture the fragmentation in the Pop III star forming halos.

### 3.3. The formation rate of $\text{H}_2$

Since the onset of the chemothermal instability is strongly associated with the formation of hydrogen molecules, it is therefore instructive to examine the rate at which  $\text{H}_2$  actually forms in the collapse calculations.

We calculate the  $\text{H}_2$  formation rate ( $dn_{\text{H}_2}/dt$ ) from the data generated in our simulations and plot as a function of density in Figure 1C. To create these plots, we first calculate the number density of hydrogen molecules on a mass shell that has a particular density and temperature for a specific epoch (i.e., for a given snapshot at time  $t_1$ ). For the same snapshot, we then keep on calculating the number density of hydrogen molecules for different mass shell (each of which has a particular density and temperature). Both the density and temperature are radially-logarithmic binned, mass-weighted averages. We repeat the procedure for the consecutive snapshot of time  $t_2$ . We compare the  $\text{H}_2$  abundances in these snapshots from the simulations over a time interval  $\Delta t = t_2 - t_1$ , with the rates given by

$$\frac{dn_{\text{H}_2}}{dt} = \frac{n_{\text{H}}(t_2)y_{\text{H}_2}(t_2) - n_{\text{H}}(t_1)y_{\text{H}_2}(t_1)}{t_2 - t_1}. \quad (5)$$

Note that an assumption here is made that the number density of the gas between the two snapshots does not

change significantly and the time interval  $\Delta t$  is chosen as small as possible ( $\approx 8$  months, considerably small compared to both the free-fall and cooling times).

Over the range of densities in which the three-body reactions are important (i.e. above  $10^7 \text{ cm}^{-3}$ ), we find that the differences in  $dn_{\text{H}_2}/dt$  between the simulations are strongly density dependent. Around a density of  $\sim 10^8 - 10^9 \text{ cm}^{-3}$ , the difference between the formation rates in the simulations is the highest. The curve is steeper in this regime, allowing us to infer that the rapid production of hydrogen molecules can cool the gas promptly and hence trigger the cooling time to be shorter than the free-fall time.

Note that at high densities this method is no longer strictly applicable as it is highly sensitive to the chosen time interval. However, this calculation provides a good estimate for the overall trend of the rate of  $\text{H}_2$  formation inside the haloes in which we are particularly interested.

### 3.4. Fragmentation and long term evolution

Fragmentation can be manifested in various terms, as it depends on the thermal and chemical history, interaction with the surroundings, gas mass and instability in the clouds. Here we focus on how the thermo-dynamical evolution due to the heating and cooling rates can provide a hint of future fragmentation in our calculations.

One can measure the instability in the gas by computing the number of Jeans mass, or more appropriately the Bonnor-Ebert mass ( $M_{\text{BE}}$ ) inside the central dense volume (Ebert 1955; Bonnor 1956). This is same as comparing the fragmentation timescale ( $t_{\text{frag}}$ ) with the accretion timescale ( $t_{\text{acc}}$ ). In other words, the ratio,  $t_{\text{frag}}/t_{\text{acc}}$ , is equivalent to the ratio,  $M_{\text{BE}}/\dot{M}$ , i.e., the inverse of the number of Bonnor-Ebert mass masses enclosed in the central volume. We define the fragmentation timescale as the rate of change in the number  $M_{\text{BE}}$  within a given radial shell (Dopcke et al. 2013),

$$t_{\text{frag}} \equiv \frac{M_{\text{BE}}}{\dot{M}}, \quad (6)$$

and compare it with the accretion timescale (Abel et al. 2002), defined as

$$t_{\text{acc}} = \frac{M_{\text{enc}}(r)}{4\pi r^2 v_{\text{rad}} \dot{M}}, \quad (7)$$

where  $\dot{M}$ ,  $M_{\text{enc}}$ , and  $v_{\text{rad}}$  are the mass accretion rate, enclosed mass and radial velocity, respectively. The results are shown in Figure 1D. The snapshots were taken just before the formation of the first protostar. The dashed lines represent the case when fragmentation timescale is equal to the accretion timescale.

If  $t_{\text{frag}}/t_{\text{acc}} > 1$ , the gas enclosed in the shells is accreted faster than it can fragment. As a result, fewer new protostars are formed and the available mass contributes to the mass growth of the existing ones. In our case, we find  $t_{\text{frag}}/t_{\text{acc}} < 1$ , i.e., the gas in the shells can fragment faster than it is accreted by the central dense clump, favouring low-mass protostars. Therefore, comparing only the timescale, we get an indication of the possible fragmentation from the thermo-dynamical evolution of the gas before the onset of the sink formation.

At later epochs, we follow the simulations for  $\approx 3500 - 6500 \text{ yr}$  (depending on the cosmic variance of the



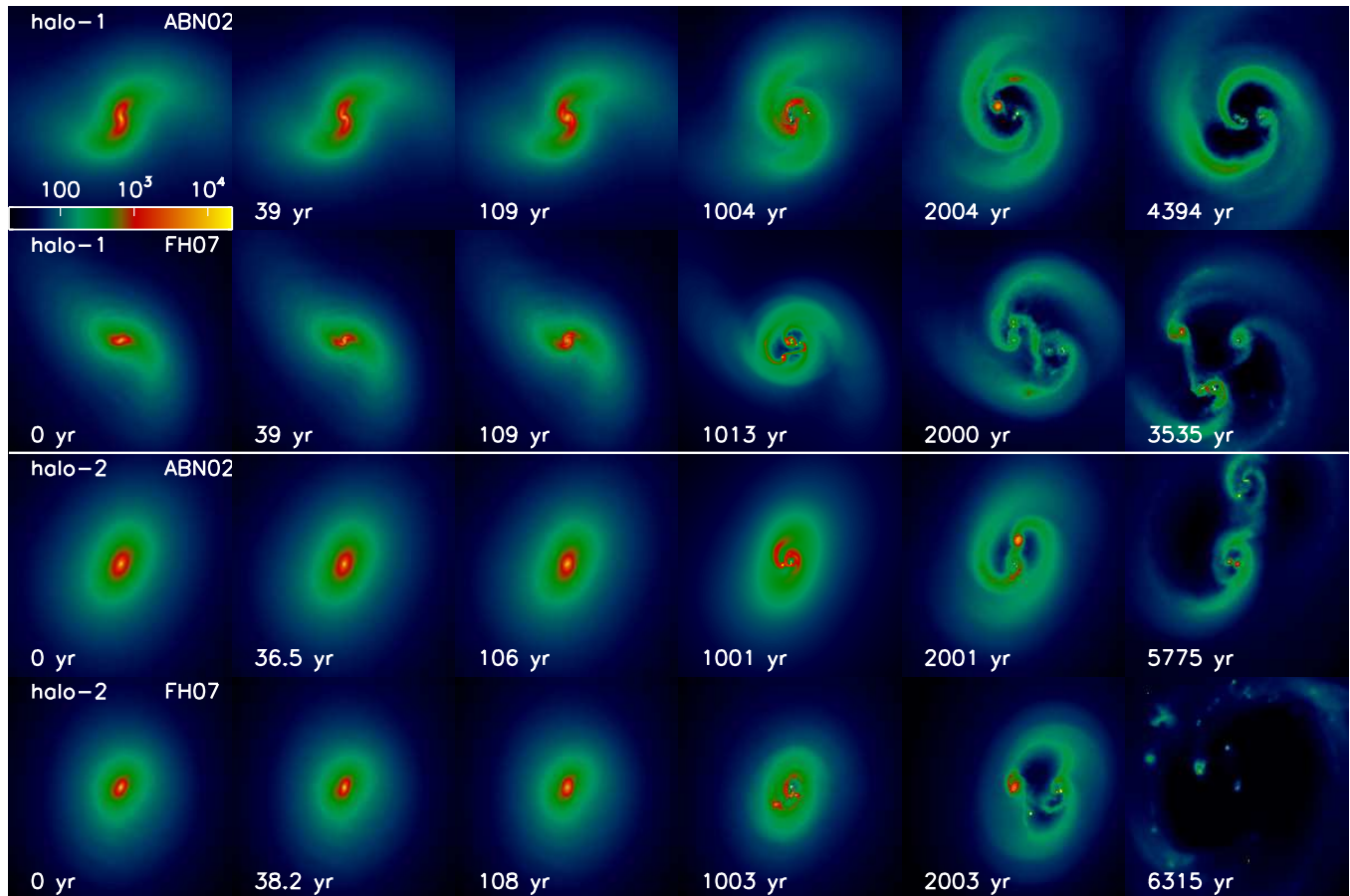


FIG. 2.— Evolution of surface density in the disk at later epochs in a region of 2000 AU centred around first protostar in the cosmological minihaloes for different proposed three-body  $H_2$  formation rates.

minihaloes) after the formation of the first sink particle. The column density in the inner 2000 AU at the end of the simulations are shown in Figure 2. In all cases we see that the simulations exhibit the disk structure that fragments on several scales within this central region. We can also see that the density in the disk are slightly less in the case with the FH07 rate due to the increased  $H_2$  fraction. The disk evolves with time with the matter accreted on to sink particles, and becomes more and more Jeans unstable.

We conclude that the temperature continues to rise with increasing density meaning that there is no preferred scale at which fragmentation takes place during the collapse. Any future fragmentation is likely to be a result of the drop in the Jeans mass that is a strong function of temperature. Hence the intricate combination of the heating and cooling rates during the three-body reaction plays a significant role in determining the unstable clumps in the cloud.

#### 4. SUMMARY

We have investigated the diverse cooling and heating mechanism in two cosmological minihaloes during the gas collapse to higher density. We have compared the physical processes with the extreme three-body formation rate coefficients proposed by Abel et al. (2002) and by Flower & Harris (2007).

We argue that although the quantity  $t_{\text{cool}}/t_{\text{ff}}$  might determine the onset of the chemothermal instability, the increase in the  $H_2$  cooling throughout the fully molecular

gas is offset by  $H_2$  formation heating with compressional heating. Hence the thermal instability need not necessarily be the criterion for possible fragmentation. Rather, the thermo-dynamical evolution that depends largely on the complicated combination of the heating and cooling rates develops the unstable clumps by affecting its Jeans mass. This leads the disk to fragment on a scale of 1000-2000 AU. However, the scale in which the fragmentation takes place depends on the three-body  $H_2$  formation rates. For example, simulations employing the ABN02 rate produce on average fewer and more massive fragments near the center, compared to those calculations using the FH07 rate (Dutta et al. 2015). However, the scale of fragmentation is comparable to the halo-to-halo variation. Our conclusion agrees well with the study by Ripamonti & Abel (2004) and Yoshida et al. (2006) that pointed that although the three-body reaction results in chemothermal instability, the growth of fluctuations are too small to lead to any fragmentation. Despite considerable computational efforts involved, we emphasize here that we cannot rule out the plausible concept of the chemothermal instability as the sole reason in all Pop III disk fragmentation scenarios. This is because of the fact that we have only considered two realizations. It is therefore of immediate interest to investigate the chemothermal instability in a number of minihaloes, like those in Hirano et al. (2014).

In summary, we have explicitly shown various heating and cooling rates in a 3D simulation of Pop III col-

lapse. This unique approach to the problem enables us to conclude that the fragmentation behavior does not necessarily happen due to the chemothermal instability. Instead, fragmentation occurs when  $H_2$  cooling, the heat released by  $H_2$  formation, and  $p dV$  compressional heating together set the Jeans mass in the gas to values that are conducive to breakup and collapse.

The author is grateful to Prateek Sharma, Agnieszka Janiuk, B. N. Dwivedi, Biman Nath, Dominik Schleicher, John Wise and Jarrett Johnson for thoroughly checking the manuscript and efficacious comments. The author

acknowledges the referee for helpful suggestions that have helped to ameliorate the clarity of the paper. The author is supported by the Indian Space Research Organization grant (No. ISRO/RES/2/367/10-11) to Banibrata Mukhopadhyay and Department of Science and Technology (DST) grant (Sr/S2/HEP-048/2012) to Prateek Sharma. The author would also like to thank the Department of Physics, Indian Institute of Technology (Banaras Hindu University) at Varanasi and the Inter-University Center for Astronomy and Astrophysics at Pune for the local hospitality.

## REFERENCES

- Abel, T., Bryan, G. L., & Norman, M. L. 2002, *Science*, 295, 93
- Barkana, R., Loeb, A., 2001, *Phys. Rep.*, 349, 125
- Bate, M. R., Bonnell, I. A. & Price, N. M. 1995, *MNRAS*, 277, 362
- Bate, M. R., Burkert, A., 1997, *MNRAS*, 288, 1060 B
- Bromm, V., Coppi, P. S., & Larson, R. B., 2002, *ApJ*, 564, 23
- Bromm, V., & Larson, R. B. 2004, *ARA&A*, 42, 79
- Bromm, V., Yoshida, N., 2011, *ARA&A* 49, 373
- Bromm, V., 2013, *RPPh*, 76k2901B
- Bonnor, W., B. 1956, *MNRAS*, 116, 351
- Ebert, R., Z. 1955, *Astrophys. J.*, 217
- Ciardi, B. & Ferrara A. 2005, *Space Sci. Rev.*, 116, 625
- Clark, P. C., Glover, S. C. O., Klessen, R. S. & Bromm, V. 2011a, *ApJ* 727 110
- Clark, P. C., Glover, S. C. O., Smith, R. J., Greif, T. H., Klessen, R. S. & Bromm, V. 2011b, *Science*, 331, 1040
- Dopcke, G.; Glover, S. C. O.; Clark, P. C.; Klessen, R. S., 2013, *ApJ*, 766, 103D
- Dutta, J; Nath, B. B.; Clark, P. C.; Klessen, R. S., 2015, *MNRAS*, 450, 202D
- Dutta, J., 2015, Accepted to the *A&A*
- Flower, D. R., & Harris, G. J. 2007, *MNRAS*, 377, 705
- Glover, S. C. O., & Abel, T. 2008, *MNRAS*, 388, 1627
- Glover, S. C. O. & Savin, D. W., 2009, *MNRAS*, 393, 911
- Glover, S. 2013, *ASSL*, 396, 103G
- Greif, T. H.; Springel, V.; White, S. D. M.; Glover, S. C. O.; Clark, P. C.; Smith, R. J.; Klessen, R. S.; Bromm, V., 2011, *ApJ*, 737, 75G
- Greif, T. H.; Bromm, V.; Clark, P. C.; Glover, S. C. O.; Smith, R. J.; Klessen, R. S.; Yoshida, N.; Springel, V. 2012, *MNRAS*, 424, 399G
- Greif, T. H.; Springel, V.; Bromm, V. 2013, *MNRAS*, 434, 3408G
- Haiman, Z.; Thoul, A. A.; Loeb, A. 1996, *ApJ*, 464, 523H
- Hirano, S.; Hosokawa, T.; Yoshida, N.; Umeda, H.; Omukai, K.; Chiaki, G.; Yorke, H., 2014, *ApJ*, 781, 60H
- Hirano, S.; Hosokawa, T.; Yoshida, N.; Omukai, K.; Yorke, H., 2015arXiv150101630H
- Hartwig, T.; Clark, P. C.; Glover, S. C. O.; Klessen, R. S.; Sasaki, M., 2015, *ApJ*, 799, 114H
- Jappsen, A.-K., Klessen, R. S., Larson, R. B., Li, Y., & Mac Low, M.-M. 2005, *A&A*, 435, 611
- Johnson, J. L.; Dalla V. C; Khochfar, S., 2013, *MNRAS*, 428, 1857J
- Krumholz, M. R., McKee, C. F. & Klein, R. I., 2004, *ApJ*, 611, 399
- Latif, M. A.; Schleicher, D. R. G., 2015, *MNRAS*, 449, 77L
- Omukai, K., & Nishi, R. 1998, *ApJ*, 508, 141
- Omukai, K., 2000, *ApJ*, 534, 809-824
- Omukai K., Yoshii Y., 2003, *ApJ*, 599, 746
- Omukai, K., Tsuribe, T., Schneider, R., & Ferrara, A. 2005, *ApJ*, 626, 627
- Palla, F., Salpeter, E. E., & Stahler, S. W. 1983, *ApJ*, 271, 632
- Planck Collaboration Ade P. A. R., Aghanim N., Armitage Caplan C., Arnaud M., Ashdown M., Atrio-Barandela F., Aumont J., Baccigalupi C., Banday A. J., et al. 2014, *A&A*, 571, A16
- Ripamonti, E., & Abel, T. 2004, *MNRAS*, 348, 1019
- Sabano Y., Yoshii Y., 1977, *PASJ*, 29, 207
- Silk J., 1983, *MNRAS*, 205, 705
- Smith, R. J.; Glover, S. C. O.; Clark, P. C.; Greif, T.; Klessen, R. S., 2011, *MNRAS*, 414, 3633S
- Susa, H.; Uehara, H.; Nishi, R.; Yamada, M., 1998, *PThPh*, 100, 63S
- Springel, V., 2005, *MNRAS*, 364, 1105
- Springel, V., 2010, *MNRAS*, 401, 791S
- Stacy, A., Greif, T. H., & Bromm, V. 2010, *MNRAS*, 403, 45
- Stacy, A., Greif, T. H., Klessen, R. S., Bromm, V. & Loeb, A., 2013, *MNRAS*, 431, 1470S
- Tegmark, M.; Silk, J.; Rees, M. J.; Blanchard, A.; Abel, T.; Palla, F., 1997, *ApJ*, 474, 1T
- Turk, M. J., Abel, T., & O'Shea, B. W. 2009, *Science*, 325, 601
- Yoshida, N., Omukai, K., Hernquist, L., & Abel, T. 2006, *ApJ*, 652, 6
- Yoshida, N., Omukai, K., & Hernquist, L. 2008, *Science*, 321, 669